Published in final edited form as:
Nano Lett. 2011 March 9; 11(3): 1306–1312. doi:10.1021/nl104378f.

Nanolithographic control of the spatial organization of cellular adhesion receptors at the single-molecule level

Mark Schvartzman[1,5,a], **Matteo Palma**[2,3,5], **Julia Sable**[4,5], **Justin Abramson**[3,5], **Xian Hu**[6], **Michael P. Sheetz**[4,5], and **Shalom J. Wind**[2,5]

[1]Department of Chemical Engineering, Columbia University, 500 West 120th St., New York, NY 10027

[2]Department of Applied Physics and Applied Mathematics, Columbia University, 500 West 120th St., New York, NY 10027

[3]Department of Mechanical Engineering, Columbia University, 500 West 120th St., New York, NY 10027

[4]Department of Biological Sciences, Columbia University, 1212 Amsterdam Ave., New York, NY 10027

[5] Nanomedicine Center for Mechanobiology – Directing the Immune Response, Columbia University, New York, NY 10027

[6]Department of Biological Sciences National University of Singapore

Abstract

The ability to control the placement of individual molecules promises to enable a wide range of applications and is a key challenge in nanoscience and nanotechnology. Many biological interactions, in particular, are sensitive to the precise geometric arrangement of proteins. We have developed a technique which combines molecular-scale nanolithography with site-selective biochemistry to create biomimetic arrays of individual protein binding sites. The binding sites can be arranged in heterogeneous patterns of virtually any possible geometry with a nearly unlimited number of degrees of freedom. We have used these arrays to explore how the geometric organization of the extracellular matrix (ECM) binding ligand RGD (Arg-Gly-Asp) affects cell adhesion and spreading. Systematic variation of spacing, density and cluster size of individual integrin binding sites was used to elicit different cell behavior. Cell spreading assays on arrays of different geometric arrangements revealed a dramatic increase in spreading efficiency when at least 4 liganded sites were spaced within 60 nm or less, with no dependence on global density. This points to the existence of a minimal matrix adhesion unit for fibronectin defined in space and stoichiometry. Developing an understanding of the ECM geometries that activate specific cellular functional complexes is a critical step toward controlling cell behavior. Potential practical applications range from new therapeutic treatments to the rational design of tissue scaffolds that can optimize healing without scarring. More broadly, spatial control at the single-molecule level can elucidate factors controlling individual molecular interactions and can enable synthesis of new systems based on molecular-scale architectures.

*Corresponding author: Shalom J. Wind, Department of Applied Physics and Applied Mathematics, Columbia University, 530 West 120th St., MC 8903, New York, NY 10027 Tel. 212-854-5122 Fax: 212-854-1909 sw2128@columbia.edu.
[a]Present address: Department of Materials Chemistry, Weizmann Institute of Science, Rechovot, Israel

Keywords

nanofabrication; nanobiology; mechanobiology; integrin clustering; cell adhesion

The extraordinary growth of the electronics industry over the past four decades has been fueled by the scaling of transistor features defined by lithographic patterning. In recent years, semiconductor lithography techniques have begun to see use in biological and medical applications ranging from DNA microarrays[1,2] and protein chips[3,4] to devices for measuring cellular mechanics.[5-8] By and large, most of these devices comprise features in the micron scale – approximately where semiconductor technology was in the mid-1980's. Current state-of-theart lithographic processes are capable of achieving ~ 30 nm resolution.[9] Among the candidates for future generation lithography technologies is nanoimprint lithography (NIL),[10,11] which is a high throughput patterning technique in which a pattern is formed in a thin polymer film that has been cast on a substrate by molding it to a relief image in a rigid template (mask). The pattern is then transferred from the polymer by a variety of thin film deposition and/or etching techniques. There is no theoretical limitation to the resolution of the features imprinted by NIL;[12] the practical limit is determined by the size of the features on the NIL template, which is typically patterned by electron beam lithography. We have recently developed a process based on NIL and self-aligned pattern transfer which reduces the imprinted feature size and is capable of creating metallic structures below 5 nm.[13] We have also developed a facile surface chemistry which allows us to functionalize these structures with a broad array of biomolecular species with a high degree of selectivity.[14] Using these techniques, we have fabricated biomimetic surfaces upon which we can control the precise placement of individual biomolecules. We report here how these surfaces can be used to study the role of geometric organization of extracellular matrix (ECM) binding ligands in controlling cell adhesion and spreading.

Cells interact with the extracelluar matrix (ECM) via integrins, which are transmembrane receptors linking the ECM to macromolecular complexes that bind to the actin cytoskeleton, forming adhesive contacts.[15] Integrin-mediated interactions with matrix control cell adhesion and migration and play a central role in many developmental and functional processes in multicellular organisms, including differentiation, wound healing and metastasis.[16,17] They are also important for drug design and tissue engineering. Adhesive contacts are stabilized by the binding of talin to integrin cytoplasmic domains, followed by reinforcement and activation of other proteins such as paxillin, vinculin and α-actinin.[18] Different integrins bind to different ECM ligands, although the RGD (Arg-Gly-Asp) peptide sequence has been recognized as the main adhesive recognition site within the cell-binding region of fibronectin.[16,19,20]

Establishing the minimal requirements for adhesion has been a goal of researchers for many years. Several groups have studied cell spreading and focal contact formation as a function of matrix molecule density.[21-27] Using this approach, Massia and Hubbell found that a minimum of 6 RGD ligands per micron (corresponding to a spacing of 440 nm) were sufficient to support cell spreading.[25] More recent experiments, in which the spacing of RGD ligands could be precisely controlled by micellar diblock copolymer self-assembly, [28,29] indicate that cell spreading and viability are negatively affected when the spacing between integrin binding sites exceeds ~ 60 -70 nm,[28,30] which is approximately the distance between talin1 globular head binding domains.[31] A similar spatial dependence has been observed for attachment and differentiation of neurons [32] as well as for controlling apoptosis.[33] Likewise, force-dependent measurements have shown that reliable ECM-cytoskeleton bonds could be formed only with multiple fibronectin 7-10 domains clustered within 40 – 60 nm.[34,35] In addition, cell adhesion and migration is enhanced by nanoscale

clustering of RGD domains.[36-39] An important question raised by these studies is whether or not there exists a nanometer-scale adhesive unit, defined in terms of distance and number, that supports spreading.

To determine how ligand spacing, density and number modulate ECM-cytoskeleton interactions, we used NIL to fabricate biochips (Fig. 1a) in which these factors were varied independently. Our NIL process offer significant advantages over the type of self-assembly techniques used previously in cell spreading assays,[28,30,32,33] due to its ability to form arbitrary, heterogeneous patterns of any possible geometry with a nearly unlimited number of degrees of freedom. Thus, each biochip contained several different patterns to test the effects of a variety of parameters on cell behavior simultaneously, minimizing sample-to-sample variability and making experimental results more reliable. Cell spreading assays confirmed that beyond the importance of integrin spacing, integrin cluster size was critical, independent of cluster density.

Fabrication of the nanoscale bioarray chips in this work is shown schematically in Figure 1b. Briefly, NIL templates, either from diamond-like carbon (DLC)[40-42] or hydrogen silsesquioxane (HSQ) on silicon,[43] were patterned by electron beam lithography. Pattern transfer to glass cover-slips was done by NIL into a poly-methyl methacrylate (PMMA) film, followed by residual PMMA removal and metal evaporation through an angle-evaporated hard mask,[44] lift-off and thermal annealing to obtain spherical[13] AuPd dots[45] with diameters as small as 5 nm or less.[13] Figures 1 c, d and e show high resolution SEM images of such patterns. The AuPd nanodot patterns were functionalized[14] with a mixed monolayer of thiolated polyethylene glycol (PEG) and thiolated PEG-biotin,[46] with the surrounding glass passivated against nonspecific protein binding by a PEG-silane, followed by attachment of streptavidin to the biotin groups (Fig 2a). This facilitates the binding of a broad range of molecular species. We confirmed this selective binding using a double-stranded (ds) DNA oligomer to which biotin was attached at the 5′ end. Figures 2b and 2c show fluorescent images of an array, functionalized first with Alexa-fluor488-labeled streptavidin, and subsequently with Cy3-labeled dsDNA on the same pattern, indicating the high fidelity of the process.

For our cell spreading assays, the nanodots were functionalized with biotinylated cyclic RGDfK, known for its affinity to $\alpha_V\beta_3$ and $\alpha_V\beta_5$ integrins,[47,48] through the streptavidin bridge. The unpatterned glass surface was passivated by a self-assembled monolayer of PEG in order to minimize non-specific binding of proteins to the surface.[49] While more than one streptavidin molecule (~ 4 - 5 nm[50]) may bind to a single nanodot (and more than one biotinylated RGDfk can bind to each streptavidin), each dot can accommodate only a single integrin, since the integrin head is ~ 8 – 12 nm,[51-54] providing arrays of single integrin molecule binding sites arranged in geometries defined by NIL.

All the arrays were 200 μm × 200 μm in size, providing sufficient area for the spreading of 20 - 40 3T3 fibroblast cells used in this study. In addition to the nanodots arrays, each chip contained a large area covered with a planar AuPd film with a saturated density of binding ligands. This served as a reference point for cell adhesion and spreading.

An initial test of the effect of spacing on cell spreading was done using nanodot arrays of dimers and trimers (Fig. 1c and 1d, and Fig. S2), in which the inter-dot spacing was varied in the range of 50 nm to 100 nm from array to array, while the spacing between the dimers (or trimers) in each array was kept constant to maintain the same total density of binding sites for all arrays. In addition, extended hexagonal arrays (Fig. 1f), in which the inter-dot spacing and the total RGD density were varied in a dependent fashion, were used for direct comparison to work done on arrays formed by micellar diblock copolymer self-assembly.

[28,30,55] NIH 3T3 mouse fibroblast cells were plated on the arrays, and their behavior in terms of motility and spreading was monitored simultaneously on different patterned areas. In general, the cell behavior on dimer and trimer arrays was characterized by high motility and poor adhesion and spreading. (Figures 3a, b and c show the cells on arrays of dimers, trimers, and hexagons, all with an inter-dot spacing of 60 nm, 1.5 hours after plating.) Many of the cells migrated from the dimer and trimer patterned areas to marking scribes on the glass a few tens of microns away from the edges of the arrays (Figs. 3a and b). In contrast, cells plated on the arrays of extended hexagons with inter-dot spacings 60 nm and below exhibited a high degree of adhesion and spreading (Fig. 3c), and the cells spread only within the 200 μm squares containing the nanodots. Spreading efficiency curves, which measure the percentage of spread cells as a function of time, were plotted for each array. A cell was determined to be spread[56] if (a) the cell transformed from a rounded shape to a clearly visible flat shape with microspikes and filopodia adhering to the surface, and with possible further increase in cell area; *and* (b) the cell did not return to its original unspread form at any time during the experiment, which typically ran ~ 1.5 - 3 hours. Figures 3d and e show spreading efficiency curves for arrays with various dot arrangements but with the same spacing between the neighboring dots, 50 nm and 100 nm, respectively. Spreading curves for planar AuPd are included for comparison. All the curves have a sigmoidal form, with a maximal value usually achieved in less than 1 hour. While the fastest and most complete (~ 100%) spreading occurred, as expected, on the planar AuPd, the extended hexagonal array with 50 nm inter-dot spacing appeared to provide nearly as good an environment for cell adhesion and spreading. On the other hand, the dimer and trimer arrays with the same inter-dot spacing (50 nm) exhibited a much lower percentage of spread cells, ~ 20 - 30 %, at the end of experiment. For extended hexagonal arrays with inter-dot spacings of 80 nm and 100 nm, cell behavior was similar to that observed on arrays of dimers and trimers (Fig. 3e and in Fig. S5). The surface area of the cells spread on extended hexagonal arrays with interdot spacing ≤ 60 nm was, on average, twice as high as the other arrays (Fig. S6). Because the density of RGD in the dimer and trimer patterns was much lower than in the extended hexagonal arrays, it was possible that density and not spacing was critical in determining the cell spreading efficiency for these specific types of pattern.

In order to distinguish more clearly between the roles of density and spacing in integrin binding, we designed a different pattern in which the density was allowed to vary, but the inter-dot spacing was kept constant. The pattern consisted of small heptagonal clusters with a constant inter-dot spacing of 60 nm. The distance, *a*, between clusters was varied in order to achieve a range of global densities (Fig. 4a-d). As shown in Fig. 4g, we found virtually no variation in cell spreading efficiency with available binding site density over a range from 216 dots/μm^2 (Fig. 4e) down to 51 dots/μm^2 (Fig. 4f), which corresponds to the density of binding sites in the dimer configuration that had shown poor spreading. Thus, the overall density of dots was not critical, indicating that perhaps the cluster size was playing a key role in the observed cell spreading efficiency. Such a concept has been previously proposed.[34,35,38,57-59] In fact, an analytical model developed by Irvine et al.[58] predicts strong ligand spatial distribution effects with a saturation in cluster size in the range of 3 - 4. Until now, however, it has been difficult to create a biomimetic environment in which the configuration of individual liganded binding sites could be controlled with high precision. Indeed, Arnold et al.,[60] used electron beam lithography to “subtract” areas from hexagonal close packed arrays formed by block copolymer micelle lithography to create clusters as small as 6 integrin binding sites; however they presented no data for smaller clusters.

To determine experimentally the minimum cluster size that supports spreading, we patterned arrays of clusters of 2 – 7 liganded binding sites (Fig. 5a-f). The spacing between the dots in the clusters was set at 60 nm for all the arrays, and the cluster configuration was designed to be a fragment of an extended hexagonal array. The distance, *a*, between the clusters was

varied in order to maintain a constant global density of 50 dots/μm^2 in every array, i.e., a very low density of heptagonal dot clusters (7 clusters/μm^2, Fig. 4f). When cells were plated on chips containing all these arrays, a striking increase in spreading efficiency was observed between cluster sizes of 3 and 4 (Fig. 5e). The average of multiple experiments, Fig. 5f, confirmed that there was a dramatic difference between cluster sizes of 3 or less and 4 or more at a spacing of 60 nm. Figures 5g-i show SEM images at the edge of a fixed and dried cell. Adhesive contacts can clearly be seen at the sites of the nanodot clusters.

The resolution and patterning versatility of electron beam and nanoimprint lithography facilitate the production of many different matrix arrays, thereby enabling the determination of a basic adhesion unit that can support cell spreading and adhesion. Our results suggest that such a cell spreading unit involves clustering of at least 4 liganded integrins within ~ 60 nm. Furthermore, there is no evidence that cluster size influences adhesion above the threshold of 4 (fig. 5e,f). The spacing between the clusters in these experiments, which was nearly 400 nm in the case of the heptagonal arrays, suggests that they are most likely inducing independent multimolecular complexes in the cells that support the spreading process. Integrin-ligand clusters would naturally have greater adhesion strength than would single molecules. High (nN) contractile forces are generated on the ECM-integrin-cytoskeleton linkages even at early times in the spreading process that could dissociate integrin-RGD bonds.[61] It is therefore reasonable to suggest that an increase in adhesion strength should correlate with an increase in spreading. Roca-Cusachs et al.[35] found that clustering can increase individual ligand adhesion strength by 7-fold, either by the recruitment of a stabilizing protein complex on the cytoplasmic end or by increasing lateral integrin interactions. In either case, clustering would reduce diffusion of integrins and their ligands after bond breakage during the spreading process, thereby promoting their reattachment and enhancing adhesion. Clustering is an important part of the adhesion and spreading process, and studies of talin-depleted cells have shown that longer term spreading requires talin binding.[62] Notably, talin is a dimeric, integrin-binding protein that has 4 potential integrin binding sites.[31] Thus, we suggest that there is a discrete multimolecular adhesion complex involved in spreading and adhesion that requires the juxtaposition of at least 4 RGD-liganded integrins within 60 nm, and involves talin.

In earlier studies with constructs of fibronectin type-III domains formed by biochemical assembly into dimers, trimers and pentamers with 20 - 30 nm spacers,[57] the minimal cluster size for protein edge binding and bead reinforcement was found to be a trimer.[34] Our results on immobilized ligands, on the other hand, point to a minimum cluster of 4. In contrast to previous approaches, the unprecedented spatial control we have achieved over the organization of the integrin-binding RGD domains allows us to unequivocally rule out aggregation effects that can affect the size of the minimal adhesion unit. It may be that the full fibronectin domains, along with the flexibility of the linkers, could enable the multimolecular complex formation with fewer ligands per cluster.

New nanofabrication techniques combined with site-specific surface biochemical functionalization such as the one we present here enable unprecedented control over the arrangement of individual integrin molecules. We have used this strategy to identify a cell spreading adhesive unit that involves the clustering of at least 4 liganded integrins within ~ 60 nm. This finding agrees well with the established role of the cytoskeleton protein talin in cell adhesion. This approach can be generalized to enable a wide range of new studies on cellular systems and on other biomolecular interactions at the single-molecule level. They can also be used to develop new strategies in customized tissue scaffolds, wound healing bandages and cell-type-specific diagnostic and therapeutic tools.

Supplementary Material

Refer to Web version on PubMed Central for supplementary material.

Acknowledgments

We thank Pere Roca-Cusachs for helpful discussions. We gratefully acknowledge support from the National Institutes of Health through award number R01 GM076415-01 B and award number PN2EY016586 under the NIH Roadmap for Medical Research and by the National Science Foundation under award number NSF EF-05-07086. Additional support from the Nanoscale Science and Engineering Initiative of the National Science Foundation under NSF Award Number CHE-0641523 and from the New York State Office of Science, Technology, and Academic Research (NYSTAR) is also gratefully acknowledged.

References

1. Eisen MB, Brown PO. DNA arrays for analysis of gene expression. Method Enzymol. 1999; 303:179–205.
2. Fodor SPA, et al. Light-Directed, Spatially Addressable Parallel Chemical Synthesis. Science. 1991; 251:767–773. [PubMed: 1990438]
3. Houseman BT, Huh JH, Kron SJ, Mrksich M. Peptide chips for the quantitative evaluation of protein kinase activity. Nat Biotechnol. 2002; 20:270–274. [PubMed: 11875428]
4. Zhu H, Snyder M. Protein chip technology. Curr Opin Chem Biol. 2003; 7:55–63. [PubMed: 12547427]
5. Curtis A, Wilkinson C. Topographical control of cells. Biomaterials. 1997; 18:1573–1583. [PubMed: 9613804]
6. Ghassemi S, et al. Fabrication of elastomer pillar arrays with modulated stiffness for cellular force measurements. Journal of Vacuum Science & Technology B. 2008; 26:2549–2553.
7. Saez A, et al. An array of micro fabricated pillars to map forces during epithelial cell migration. Biophys J. 2005; 88:518a–518a.
8. Tan JL, et al. Cells lying on a bed of microneedles: An approach to isolate mechanical force. P Natl Acad Sci USA. 2003; 100:1484–1489.
9. The International Technology Roadmap for Semiconductors. 2009. <http://www.itrs.net/Links/2009ITRS/Home2009.htm>
10. Chou SY, Krauss PR, Renstrom PJ. Imprint of Sub-25 Nm Vias and Trenches in Polymers. Appl Phys Lett. 1995; 67:3114–3116.
11. Chou SY, Krauss PR, Renstrom PJ. Imprint lithography with 25-nanometer resolution. Science. 1996; 272:85–87.
12. Hua F, et al. Nano Letters. 2004; 4:2467.
13. Schvartzman M, Wind SJ. Robust Pattern Transfer of Nanoimprinted Features for Sub-5-nm Fabrication. Nano Letters. 2009; 9:3629–3634. [PubMed: 19722536]
14. Cherniavskaya O, et al. Fabrication and surface chemistry of nanoscale bioarrays designed for the study of cytoskeletal protein binding interactions and their effect on cell motility. J. Vac. Sci. Technol. B. 2005; 23:2972.
15. Burridge K, Chrzanowska-Wodnicka M. Focal Adhesions, Contractility, and Signaling. Annual Review of Cell and Developmental Biology. 1996; 12:463–519.
16. Geiger B, Bershadsky A, Pankov R, Yamada KM. Transmembrane crosstalk between the extracellular matrix and the cytoskeleton. Nat Rev Mol Cell Biol. 2001; 2:793–805. [PubMed: 11715046]
17. Lauffenburger DA, Horwitz AF. Cell Migration: A Physically Integrated Molecular Process. Cell. 1996; 84:359–369. [PubMed: 8608589]
18. Calderwood DA, Ginsberg MH. Talin forges the links between integrins and actin. Nature Cell Biology. 2003; 5:694–697.
19. Ruoslahti E, Pierschbacher MD. Arg-Gly-Asp - A Versatile Cell Recognition Signal. Cell. 1986; 44:517–518. [PubMed: 2418980]

20. Ruoslahti E, Pierschbacher MD. New Perspectives in Cell-Adhesion - Rgd and Integrins. Science. 1987; 238:491–497. [PubMed: 2821619]
21. Brandley BK, Schnaar RL. Covalent Attachment of an Arg-Gly-Asp Sequence Peptide to Derivatizable Polyacrylamide Surfaces - Support of Fibroblast Adhesion and Long-Term Growth. Anal Biochem. 1988; 172:270–278. [PubMed: 3189771]
22. Danilov YN, Juliano RL. (Arg-Gly-Asp)N-Albumin Conjugates as a Model Substratum for Integrin-Mediated Cell-Adhesion. Exp Cell Res. 1989; 182:186–196. [PubMed: 2469596]
23. Hughes RC, Pena SDJ, Clark J, Dourmashkin RR. Molecular Requirements for the Adhesion and Spreading of Hamster Fibroblasts. Exp Cell Res. 1979; 121:307–314. [PubMed: 446537]
24. Humphries MJ, Akiyama SK, Komoriya A, Olden K, Yamada KM. Identification of a New, Cell Type-Specific Adhesion Signal Alternatively Spliced in Human-Plasma Fibronectin. J Cell Biol. 1986:A89–A89.
25. Massia SP, Hubbell JA. An Rgd Spacing of 440nm Is Sufficient for Integrin Alpha-V-Beta-3-Mediated Fibroblast Spreading and 140nm for Focal Contact and Stress Fiber Formation. J Cell Biol. 1991; 114:1089–1100. [PubMed: 1714913]
26. Singer II, Kawka DW, Scott S, Mumford RA, Lark MW. The Fibronectin Cell Attachment Sequence Arg-Gly-Asp-Ser Promotes Focal Contact Formation during Early Fibroblast Attachment and Spreading. J Cell Biol. 1987; 104:573–584. [PubMed: 2950119]
27. Underwood PA, Bennett FA. A Comparison of the Biological-Activities of the Cell-Adhesive Proteins Vitronectin and Fibronectin. J Cell Sci. 1989; 93:641–649. [PubMed: 2481683]
28. Arnold M, Cavalcanti-Adam EA, Glass R, Blummel J, Eck W, Kantlehner M, Kessler H, Spatz JP. Activation of Integrin Function by Nanopatterned Adhesive Interfaces. ChemPhysChem. 2004; 5:383. [PubMed: 15067875]
29. Cavalcanti-Adam EA, et al. Cell spreading and focal adhesion dynamics are regulated by spacing of integrin ligands. Biophysical Journal. 2007; 92:2964–2974. [PubMed: 17277192]
30. Cavalcanti-Adam EA, et al. Biophys. J. 2007; 92:2964. [PubMed: 17277192]
31. Critchley DR, Gingras AR. Talin at a glance. J Cell Sci. 2008; 121:1345–1347. [PubMed: 18434644]
32. Jaehrling S, Thelen K, Wolfram T, Pollerberg GE. Nanopatterns Biofunctionalized with Cell Adhesion Molecule DM-GRASP Offered as Cell Substrate: Spacing Determines Attachment and Differentiation of Neurons. Nano Letters. 2009
33. Ranzinger J, et al. Nanoscale Arrangement of Apoptotic Ligands Reveals a Demand for a Minimal Lateral Distance for Efficient Death Receptor Activation. Nano Letters. 2009
34. Jiang G, Giannone G, Critchley DR, Fukumoto E, Sheetz MP. Two-piconewton slip bond between fibronectin and the cytoskeleton depends on talin. Nature. 2003; 424:334–337. [PubMed: 12867986]
35. Roca-Cusachs P, Gauthier NC, del Rio A, Sheetz MP. Clustering of $\alpha_5\beta_q$ integrins determines adhesion strength whereas $\alpha_v\beta_3$ and talin enable mechanotransduction. Proceedings of the National Academy of Sciences. 2009; 106:16245–16250.
36. Calderwood DA, Shattil SJ, Ginsberg MH. Integrins and Actin Filaments: Reciprocal Regulation of Cell Adhesion and Signaling. Journal of Biological Chemistry. 2000; 275:22607–22610. [PubMed: 10801899]
37. Koo LY, Irvine DJ, Mayes AM, Lauffenburger DA, Griffith LG. Coregulation of cell adhesion by nanoscale RGD organization and mechanical stimulus. J. Cell Sci. 2002; 115:1423. [PubMed: 11896190]
38. Maheshawari G, Brown G, Lauffenburger DA, Wells A, Griffith LG. Cell adhesion and motility depend on nanoscale RGD clustering. J. Cell. Sci. 2000; 113:1677. [PubMed: 10769199]
39. Miyamoto S, Akiyama SK, Yamada KM. Synergistic roles for receptor occupancy and aggregation in integrin transmembrane function. Science. 1995; 267:883–885. [PubMed: 7846531]
40. Schvartzman M, Mathur A, Hone J, Jahnes C, Wind SJ. Plasma fluorination of carbon-based materials for imprint and molding lithographic applications. Appl. Phys. Lett. 2008; 93:153105. [PubMed: 19529791]

41. Schvartzman M, et al. Fluorinated diamondlike carbon templates for high resolution nanoimprint lithography. Journal of Vacuum Science and Technology B: Microelectronics and Nanometer Structures. 2008; 26:2394–2398.
42. Schvartzman M, Wind SJ. Plasma fluorination of diamond-like carbon surfaces: mechanism and application to nanoimprint lithography. Nanotechnology. 2009; 20:145306–145312. [PubMed: 19420525]
43. Gadegaard N, McCloy D. Direct stamp fabrication for NIL and hot embossing using HSQ. Microelectron. Eng. 2007; 84:2785.
44. Schvartzman M, et al. Fabrication of nanoscale bioarrays for the study of cytoskeletal protein binding interactions using nanoimprint lithography. Journal of Vacuum Science and Technology B: Microelectronics and Nanometer Structures. 2009; 27:61–65.
45. We used the alloy AuPd (40/60), which has a very small grain size, reducing agglomeration effects.
46. Mixed-thiolswere used for the formation of SAMs on the metal dots in order to ensure both an ordered packing density in the monolayer, as well as the presence of the functional biotin head group for streptavidin attachment. Pure biotinylated alkyl thiols do not assemble into ordered monolayers (Nelson, et al. Langmuir. 2001; 17:2807–2816.).
47. Boturyn D, Coll J-L, Garanger E, Favrot M-C, Dumy P. J. Am. Chem. Soc. 2004; 126:5730. [PubMed: 15125666]
48. Boturyn D, Dumy P. Tetrahedron Letters. 2001; 42:2787.
49. Suh KY, Seong J, Khademhosseini A, Laibinis PE, Langer R. Biomaterials. 2004; 25:557. [PubMed: 14585705]
50. Pugliese L, Coda A, Malcovati M, Bolognesi M. J. Mol. Bio. 1993; 231:698. [PubMed: 8515446]
51. Erb E-M, Tangemann K, Bohrmann B, Muller B, Engel J. Integrin $\alpha_{II}\beta_3$ Reconstituted into Lipid Bilayers Is Nonclustered in Its Activated State but Clusters after Fibrinogen Binding. Biochemistry. 1997; 36:7395–7402. [PubMed: 9200686]
52. Humphries MJ. Integrin structure. Biochem. Soc. Trans. 2000; 28:311–339. [PubMed: 10961914]
53. Xiong J-P, et al. Crystal Structure of the Extracellular Segment of Integrin alpha Vbeta 3. Science. 2001; 294:339–345. [PubMed: 11546839]
54. Xiong J-P, et al. Crystal Structure of the Extracellular Segment of Integrin alpha Vbeta 3 in Complex with an Arg-Gly-Asp Ligand. Science. 2002; 296:151–155. [PubMed: 11884718]
55. Glass R, Moller M, Spatz JP. Block copolymer micelle nanolithography. Nanotechnology. 2003; 14:1153–1160.
56. Bardsley WG, Aplin JD. Kinetic Analysis of cells spreading. J. Cell. Sci. 1983; 61:365. [PubMed: 6885941]
57. Coussen F, Choquet D, Sheetz MP, Erickson HP. Trimers of the fibronectin cell adhesion domain localize to actin filament bundles and undergo rearward translocation. J Cell Sci. 2002; 115:2581–2590. [PubMed: 12045228]
58. Irvine DJ, Hue KA, Mayes AM, Griffith LG. Simulations of cell-surface integrin binding to nanoscale-clustered adhesion ligands. Biophysical Journal. 2002; 82:120–132. [PubMed: 11751301]
59. Huang JH, et al. Impact of Order and Disorder in RGD Nanopatterns on Cell Adhesion. Nano Letters. 2009; 9:1111–1116. [PubMed: 19206508]
60. Arnold M, et al. Cell interactions with hierarchically structured nano-patterned adhesive surfaces. Soft Matter. 2009; 5:72–77.
61. Dubin-Thaler BJ, et al. Quantification of cell edge velocities and traction forces reveals distinct motility modules during cell spreading. PLoS One. 2008:e3735. [PubMed: 19011687]
62. Zhang X, et al. Talin depletion reveals independence of initial cell spreading from integrin activation and traction. Nat Cell Biol. 2008; 10:1062–1068. [PubMed: 19160486]

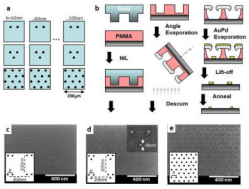

Figure 1.

a Schematic view of a biochip containing arrays of sub-10 nm functionalized nanodots, arranged in dimers, trimers and extended hexagons with various inter-dot spacings. Each pattern extends over an area of 200 microns. **b**, Schematic fabrication process flow of AuPd nanodot arrays. **c-e.** SEM of arrays of dimers, trimers and extended hexagons, respectively.

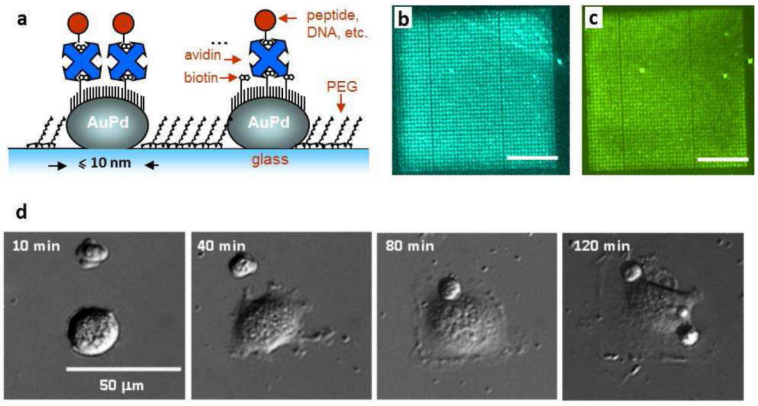

Figure 2.

a Biofunctionalization scheme of AuPd nanodots. **b**. Fluorescence imaging of a dimer array functionalized with Alexa-fluor 488-labeled neutravidin. **c**. Fluorescence imaging of a the same array after the conjugation of Cy3-labelled dsDNA (570 nm) to neutravidin. It should be noticed that the DNA imaging is shown here only to demonstrate the feasibility of the used functionalization process. For all the cell experiments described in this paper, biotinylated cyclic RGDfk was used as the final conjugated peptide agent. The scale bar in **b** and **c** is 15 micron. **d.** A cell spreading on a single rectangular pattern field. The cell conforms to the area of the pattern.

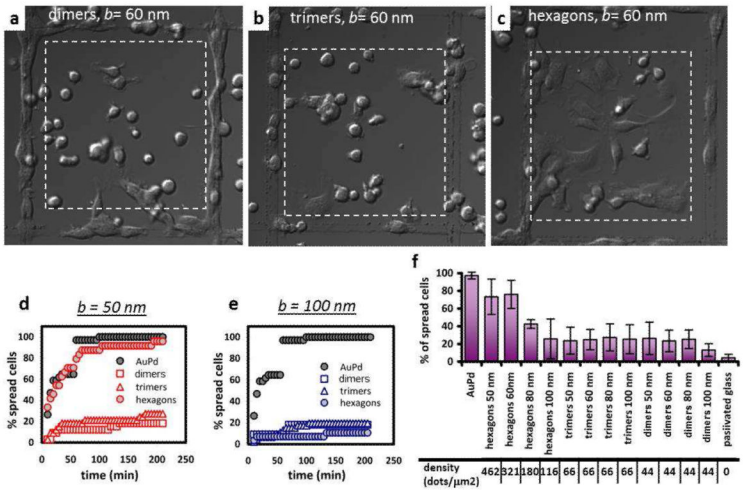

Figure 3.

a-c. 3T3 cells spread on arrays of dimers, trimers and extended hexagons respectively, with b = 60 nm. Area enclosed by boxes is 200 μm × 200 μm. **d**. Cell spreading efficiency for different arrays with b = 50 nm. **e**. Cell spreading efficiency for different arrays with b = 100 nm. **f**. Average values of spreading efficiency for the arrays tested.

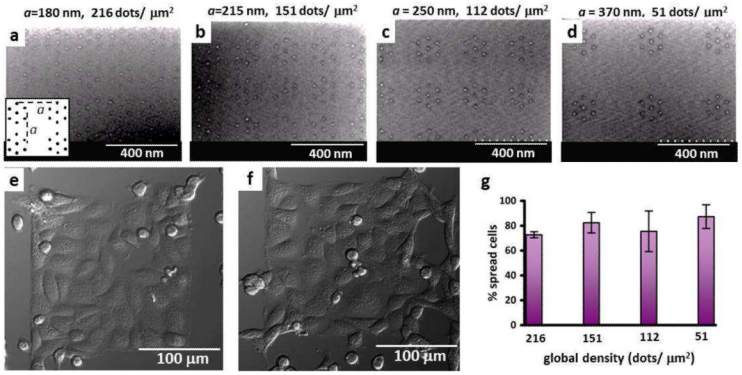

Figure 4.

a-d. SEM of arrays of nanodots, arranged in heptagonal clusters. **e,f**. 3T3 cells spread on arrays of heptagonal clusters with a = 180 nm (global density of 216 dots/mm^2) and a = 370 nm (global density of 51 dots/mm^2), respectively. **g**. Average values of spreading efficiency for heptagonal cluster arrays.

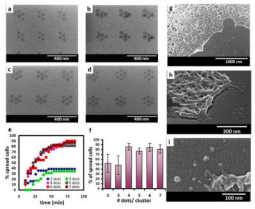

Figure 5.
a-d. SEM of arrays of nanodots, arranged in clusters of 4, 5, 6, and 7, respectively. **e**. An example of spreading curves obtained from a biochip with arrays of clusters of 2 -7 dots. **f**. Average values of spreading efficiency for the tested arrays with different clusters. **g-i**. SEM images of spread cells on arrays of heptagonal clusters.